10.2514/6.2016-5441

AIAA SPACE Forum
13 - 16 September 2016, Long Beach, California
AIAA/AAS Astrodynamics Specialist Conference

Trajectory Optimization for a Mars Ascent Vehicle

Joel Benito[1]
Jet Propulsion Laboratory, California Institute of Technology, Pasadena, CA 91109 USA

and

Breanna J. Johnson[2]
University of Michigan, Ann Arbor, MI 48109 USA

The trajectory design, propellant loading, and staging of a Mars Ascent Vehicle (MAV) can be accomplished via the solution of the associated optimal control problem under given vehicle, mission, path and control constraints. This paper presents the implementation of this optimization using Gauss Pseudospectral OPtimization Software (GPOPS-II) in combination with a Sparse Nonlinear OPTimizer (SNOPT) as the nonlinear programing solver. The solution obtained is an input to the propulsion, Guidance Navigation and Control, mechanical design, aerodynamic and thermal analysis teams, which use it to size systems, tune algorithms and update models. Optimal solutions are obtained for a variety of MAV architectures, which can be grouped in categories according to the number of stages (one or two) and the propulsion technology (solid, liquid or hybrid). A sensitivity analysis of variables of interest, like launch conditions, target orbit, stage and payload mass is presented.

I. Introduction

LAUNCH vehicle design is tightly coupled to trajectory design. Although this is true for all vehicles, it is of special importance for launch vehicles, which possess large gear ratios between each additional dry mass increment and the liftoff mass. This means that every change to the launch vehicle design impacts the vehicle's ability to meet trajectory path constraints and that changes in path constraints affect vehicle design. Additionally, designing a light launch vehicle for Mars, a Mars Ascent Vehicle (MAV), is critical due to the fact that the vehicle has to previously be landed on Mars with enough mass allocation to account for a Martian sample. Ensuring that there is enough margin for this payload is necessary to accomplish the mission of placing a rock sample into Martian orbit before another vehicle would bring this sample to Earth. Each kilogram of the Martian sample requires a few kilograms of container mass. This additional mass would then need more structural and propellant mass to lift. A heavier MAV affects not only the Martian launch trajectory design, but also has broader mission design repercussions. Every additional kilogram to a MAV would also add a few kilograms to the launch support systems. Additions to a MAV and its associated launch support system would then demand for a heavier Mars entry vehicle and a heavier, more powerful, Earth launch vehicle. With this growth in mind, the coupled vehicle-trajectory design must account for how dry mass growth affects vehicle system characteristics, like propulsion and aerodynamic constraints.

In order to accomplish the lightest possible MAV, the trajectory and vehicle should be optimized. Different optimization options are available. Techniques based on constrained optimal control [1-3] do not address the staging and vehicle design aspects of the problem, since they typically assume a given initial mass and attempt to maximize the final mass (hence to minimize propellant usage). Alternate options employ a user defined control parameterization, which can then be optimized by using standard parameter optimization algorithms like genetic algorithms or gradient descent. For example, the Space Shuttle ascent guidance algorithm [4] uses an atmospheric ascent profile optimized and obtained before flight that is executed open-loop. These options do not address the coupled vehicle-trajectory optimization and require assumptions on the trajectory that can only be formulated after the solutions have been correctly characterized. In an open design space, a general yet flexible optimization method must be used.

[1] Senior EDL Guidance and Control Engineer, Jet Propulsion Laboratory, California Institute of Technology, 4800 Oak Grove Dr., M/S 198-326, Pasadena, CA 91109, USA. Joel.Benito.Manrique@jpl.nasa.gov
[2] Aerospace Engineering Intern, Mars Program, Jet Propulsion Laboratory, California Institute of Technology, 4800 Oak Grove Dr., M/S 180-109, Pasadena, CA 91109, USA. AIAA Student Member. lunapase@umich.edu

GPOPS-II [5] offers the flexibility necessary to formulate the optimization of a multi-phase constrained dynamical system. It allows control profile and parameter optimization, which enables the solution of the multi-disciplinary problem at hand. GPOPS-II has been applied to multi-stage launch vehicle optimization [6] with success, and it is used here for different MAV designs.

The optimal trajectory and vehicle design (propellant loading per stage) obtained with GPOPS-II is used for subsequent analysis by the Guidance, Navigation and Control (GNC) team to size the Reaction Control System (RCS) and tune algorithms, by the propulsion team to adjust the propulsive dry mass, and by the mechanical team to compute the vehicle's geometry and the ground support system mass. If the trajectory and vehicle analysis provides new assumptions, the constraints and setup need to be updated and the optimization repeated.

GPOPS is a MATLAB software, and so all the results later detailed in this report stem from MATLAB code. GPOPS was employed in this paper where the user creates an input setup structure where all bounds, linkage constraints, guesses, and input parameters are defined. It is on this setup page that the user would then define the sparse linear optimizer (SNOPT) as their chosen solver for the problem.

II. Problem Formulation

The 3DOF equations of motion of an ascent vehicle are described by the following equations [1]:

$$\dot{\boldsymbol{r}} = \boldsymbol{v} \tag{1}$$

$$\dot{\boldsymbol{v}} = \boldsymbol{g} + \frac{T^i}{m}\boldsymbol{\tau} - \frac{D}{\|\boldsymbol{v_r}\|}\boldsymbol{v_r} \tag{2}$$

$$\dot{m} = -\frac{T^i}{g_0 I_{sp}^i} \tag{3}$$

$$\dot{p} = \frac{T^i}{g_0 I_{sp}^i} \tag{4}$$

where $\boldsymbol{r}$ is the position vector, in inertial frame; $\boldsymbol{v}$ is the velocity vector, in inertial frame; $\boldsymbol{g} = -\mu \boldsymbol{r}/\|\boldsymbol{r}\|^3$ is the gravity acceleration, with μ as the gravitational parameter of Mars; T^i is the thrust magnitude for stage *i*, which can be time varying if added as a control; $\boldsymbol{\tau}$ is the unit thrust direction vector, in inertial frame; D is the atmospheric drag acceleration; $\boldsymbol{v_r} = \boldsymbol{v} - \boldsymbol{\Omega} \times \boldsymbol{r}$ is the planet-relative velocity (we will assume the absence of winds, thus it is equivalent to the atmosphere relative velocity) with $\boldsymbol{\Omega}$ the planet rotation rate vector; m is the vehicle mass; $g_0 = 9.80665\ m/s^2$ is the reference acceleration; I_{sp}^i is the specific impulse of stage *i*. For Single Stage To Orbit (SSTO) architectures, the superscript *i* designates the burn number. Drag acceleration takes the standard form:

$$D = \bar{q}\frac{S}{m}C_D \tag{5}$$

where $\bar{q} = 1/2\,\rho\|\boldsymbol{v_r}\|^2$ is the dynamic pressure, ρ is the atmospheric density, S is the reference aerodynamic surface, and C_D is the aerodynamic drag coefficient. The model shown uses a drag-only aero model, which is a good approximation, given the low values of the lift coefficient and angles of attack during the trajectory.

The state variable p in Eq. (4) corresponds to the amount of propellant used along the trajectory. With a fixed initial condition p(0)=0, this variable will be used to constrain the dry mass, which is a function of the propellant.

The optimization objective is to minimize the Gross Liftoff Mass (GLOM) with the cost function:

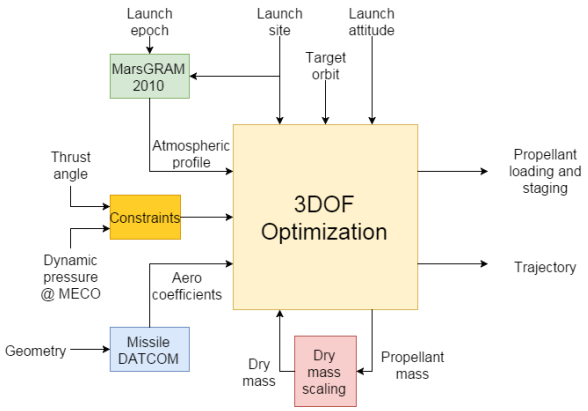

Figure 1. Optimization setup block diagram.

$$J = m(0) \tag{6}$$

by modulating the control (thrust direction $\boldsymbol{\tau}$), the propellant loading per stage/burn, and the duration of each of the phases in which the ascent is divided; all while satisfying a series of initial, terminal, path and event constraints. The phases and constraints are defined in the following Section. Figure 1 shows the block diagram of the optimization process.

III. MAV Mission and Vehicle Constraints

We divide the ascent trajectory into five phases: launch, first burn, first coast, second coast and second burn. See Fig. 2 for a graphical description of the phases.

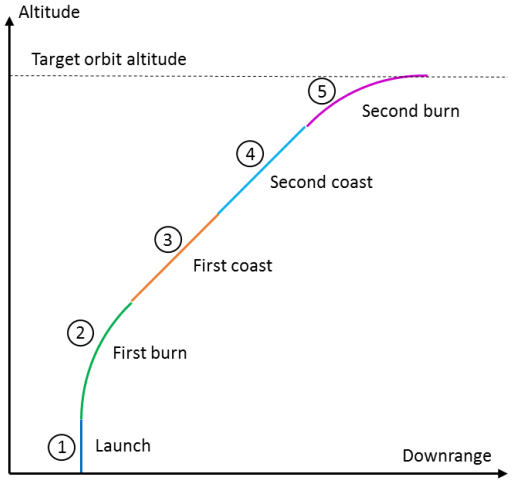

Figure 2. Schematic (not to scale) showing the different phases.

A. First Phase: Launch

The launch phase has a constant duration, typically set by hand, and is a function of the thrust-to-weight ratio of the vehicle: long enough to ensure the vehicle is at least two vehicle lengths in altitude. This is done to ensure adequate clearance from the launch site before closed-loop translational guidance is initiated. During this phase the thrust vector $\boldsymbol{\tau}$ is constant and is computed as a function of the desired launch elevation and azimuth. Launch elevation and azimuth are defined as optimization parameters, which can be constrained to a specific value or left free so the optimizer obtains the best value to minimize GLOM, as it will be shown in the next section. Given an elevation angle ε and an azimuth angle ψ (counter-clockwise from East), the thrust direction is computed by:

$$\boldsymbol{\tau_1} = R_z(-\theta)R_y(\phi)R_x(-\psi)R_z(\varepsilon - \pi/2)\,[1 \quad 0 \quad 0]^T \tag{7}$$

where θ is the liftoff longitude and ϕ is the liftoff latitude. R_x, R_y and R_z are the rotation matrices in the *x*, *y* and *z* directions respectively.

The initial position, constrained to $\boldsymbol{r}(0) = \boldsymbol{r_0}(\theta_0, \phi_0, h_0)$, is given by the launch longitude, latitude, and altitude above the reference radius. In this phase there is no control, and the phase duration is fixed by $t_1^f = t_{launch}$. Thrust direction is given by $\boldsymbol{\tau_1}$ in Eq. (7). There is the initial constraint $\boldsymbol{v_r}(0) = \boldsymbol{\tau_1}\|\boldsymbol{v_r}(0)\|$, which requires a nonzero $\|v_r(0)\|$, set to 1 mm/s. The parameters launch elevation and azimuth are constrained to $\varepsilon_{min} \leq \varepsilon \leq \varepsilon_{max}$ and $\psi_{min} \leq \psi \leq \psi_{max}$. For the results in this paper the launch is vertical, therefore $\varepsilon_{min} = \varepsilon_{max} = \pi/2$ and $\psi_{min} = \psi_{max} = 0$. Relaxing the constraint on elevation and azimuth would allow the optimizer to find the best launch attitude to minimize GLOM.

B. Second Phase: First Burn

The second phase, the first burn phase, has to satisfy two path constraints. The first constraint is $\|\boldsymbol{\tau}(t)\| = 1$, ensuring that the thrust vector has unit magnitude. The second constraint attempts to limit the maximum angle of attack, which should be limited to minimize aerodynamic torques and therefore minimize the attitude control effort. Since the 3DOF equations of motion are translational only, and model the vehicle as a point-mass, there is no rotational information and therefore the angle of attack is not defined. As a proxy for angle of attack, we define the thrust angle, or angle between the thrust vector and the planet-relative velocity:

$$\Gamma(t) = \operatorname{acos}\left(\frac{\boldsymbol{\tau}(t) \cdot \boldsymbol{v_r}(t)}{\|\boldsymbol{v_r}(t)\|}\right) \tag{8}$$

Although the thrust direction does not generally align with the vehicle axis, the thrust angle deflection in the body frame cannot be large, due to limits in the thrust vector control system. Excursions from the centerline are temporary to orient the vehicle, based on the reasonable assumption that the vehicle's center of mass is in the body axis. Therefore, we can use the approximation $|\alpha| \approx \Gamma$ with confidence, with the caveat that during the coast phases, with

no thrust vector defined, the thrust angle is not defined either. The second path constraint is finally $\Gamma(t) \leq \Gamma_{max}$, with no need to specify the absolute value because Γ is defined positive by Eq. (8).

In order to limit the aerodynamic torques after Main Engine Cut-Off (MECO), a terminal constraint in phase two is introduced that constrains the dynamic pressure to a specified maximum value: $\bar{q}(t_2^f) \leq \bar{q}_{max}^{MECO}$, where t_2^f is the final time of phase two. During the burn there are large amounts of attitude control authority thanks to the large main engine thrust and a large moment arm. After MECO, however, all attitude control is performed using cold gas thrusters. The lower the thrust of the RCS thrusters, the lower the dry mass, and the lower the GLOM. By limiting the dynamic pressure at MECO (which is also the largest dynamic pressure during coast), the size of the RCS thrusters is also limited, possibly with a propellant usage penalty.

C. Third and Fourth Phases: Coast

During these phases the vehicle is ascending to apoapse and there is no applied thrust. No path constraints are enforced. The duration for phase three is fixed, and set by hand in order to have two coast phases of similar duration. Having two coast phases is unnecessary and introduces tens of constraints to the optimization problem. The additional coast phase is introduced to provide the flexibility to eject a payload fairing; modeled as a mass decrease between the two coast phases. As the MAV design advanced, it was determined that a payload fairing was not necessary. However, the optimization must account for the RCS cold gas propellant allocated for attitude control during ascent. Although it is possible to model a linear drop in mass during coast, it was decided that modeling the RCS usage as a mass ejection was simpler. Therefore, the mass at the beginning of phase four is constrained to:

$$m(t_4^0) = m(t_3^f) - m_{RCS} \tag{9}$$

where m_{RCS} is a fixed, given value.

For Two Stages To Orbit (TSTO) architectures, the first stage is ejected at the end of phase four, right before stage two ignition. The drop in mass is modeled by adding the following constraint:

$$m(t_5^0) = m(t_4^f) - m_{S1dry}\left(p(t_4^f)\right) \tag{10}$$

Where m_{S1dry} is the dry mass of the first stage, which is a function of the propellant used during the first burn. The simplest models use a linear approximation for the dry mass: $m_{S1dry} = m_{S1dry}^c + K_{S1}p(t_4^f)$. The function m_{S1dry} can take any form but in general it is desired to be a function as smooth and linear as possible to facilitate the optimization. In addition to Eq. (10), it is necessary to reset p so it can be used in the same way to constrain the second stage dry mass:

$$p(t_5^0) = 0 \tag{11}$$

SSTO architectures do not enforce the constraints defined in Eqs. (10) and (11).

D. Fifth Phase: Second Burn

The second burn is the circularization burn. At the beginning of this phase the vehicle has reached the apoapse of the ascent trajectory, and this phase serves to raise the periapse to end with the vehicle in Mars orbit. Similarly to the TSTO constraint for the stage ejection, the final vehicle mass has to be constrained to the expected mass given by the vehicle design and propellant used during the second burn:

$$m(t_5^f) = m_{payload} + m_{S2dry}\left(p(t_5^f)\right) \tag{12}$$

where m_{S2dry} corresponds the dry mass of the second stage for TSTO designs, or the total vehicle dry mass for SSTO designs. Two of the TSTO cases studied have an unguided upper stage, which is spun at high rpm before being fired. These unguided cases present lower GLOM, because all GNC avionics are contained in the first stage; providing a lighter second stage. The unguided second stage (phase five) is modeled by not having a control variable $\boldsymbol{\tau}(t)$ and instead computes three parameters that form a direction $\boldsymbol{\tau}_5$ in the inertial space, which are constant for the whole burn and constrained to $\|\boldsymbol{\tau}_5\|$=1. The final and most important terminal constraint is the final orbit. For the results presented in this paper, the orbital elements constrained are semi-major axis, eccentricity and inclination; leaving the rest of the elements free.

$$a\left(\boldsymbol{r}\left(t_5^f\right), \boldsymbol{v}\left(t_5^f\right), \mu\right) = a_f \tag{13}$$

$$e\left(\boldsymbol{r}\left(t_5^f\right), \boldsymbol{v}\left(t_5^f\right), \mu\right) = e_f \tag{14}$$

$$i\left(\boldsymbol{r}\left(t_5^f\right), \boldsymbol{v}\left(t_5^f\right), \mu\right) = i_f \tag{15}$$

For the case where the target orbit is circular, $e_f = 0$ and $a_f = R_p + h_{orbit}$, where R_p is the planet radius and h_{orbit} is the orbit altitude.

IV. Atmospheric and Aerodynamic Models

The atmospheric model used is MarsGRAM 2010 [7]. Prior to launching an optimization, an atmospheric profile is obtained above the designated launch site. Whereas the vehicle travels a long distance from the launch site, the distance flown while in the sensible atmosphere is small enough that we assume the atmosphere characteristics do not vary from those found above the launch site.

The drag-only aerodynamic model is obtained using Missile DATCOM [8]. Missile DATCOM allows a flexible definition of the vehicle's geometry and flight conditions explored, making it very suitable to evaluate multiple cases. Given the assumption that the vehicle is axisymmetric, only one axis needs to be explored to characterize the vehicle's aerodynamics. Missile DATCOM provides axial and normal force coefficients (C_a and C_N respectively) as a function of angle of attack and Mach number. Using the thrust angle Γ as a proxy for angle of attack, the drag coefficient in Eq. (5) is obtained by:

$$C_D(M, \Gamma) = C_a(M, \Gamma)cos\Gamma + C_N(M, \Gamma)sin\Gamma \tag{17}$$

During the coast arcs, where Γ is not defined, it is assumed that the vehicle takes a zero angle of attack attitude using the RCS thrusters, and therefore $\Gamma = 0$. The aerodynamic coefficients C_a and C_N are fitted to 2D surfaces. The functions shown in Eqs. (18)-(19) were obtained via visual inspection of the surfaces generated with data from Missile DATCOM. For each of the candidate designs, the coefficients c_i and p_{ij} are obtained using MATLAB's curve fitting toolbox.

$$C_a(M, \Gamma) = \frac{c_1 M^2 + c_2 M + c_3}{M^2 + c_4 M + c_5} + c_6 \Gamma^2 \tag{18}$$

$$C_N(M, \Gamma) = p_{00} + p_{10}M + p_{01}\Gamma + p_{11}M\Gamma + p_{02}\Gamma^2 + p_{12}M\Gamma^2 + p_{03}\Gamma^3 \tag{19}$$

Figures 3 and 4 show function fits for one of the designs under consideration.

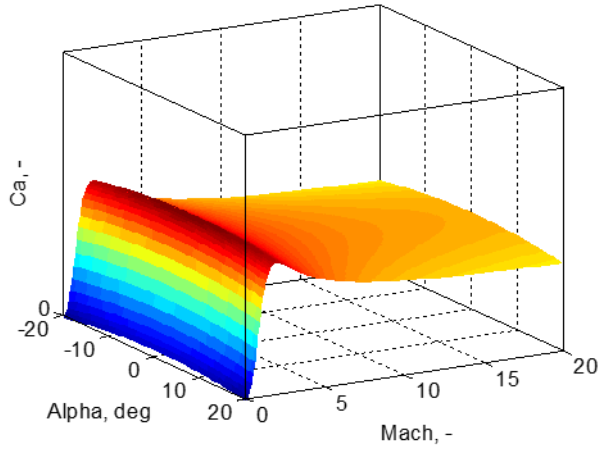

Figure 3. Axial force coefficient for a candidate MAV design.

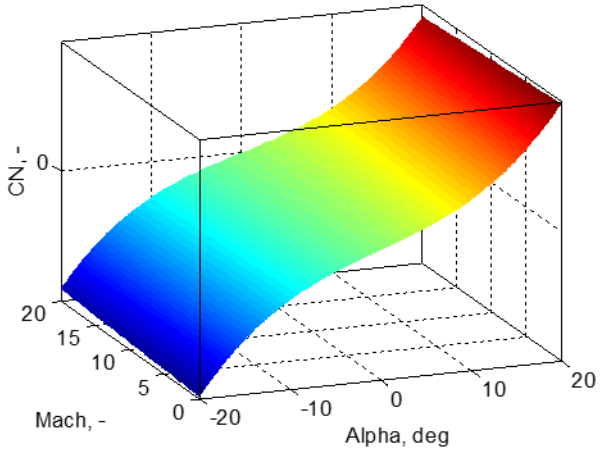

Figure 4. Normal force coefficient for a candidate MAV design.

Note that the aerodynamic data is tied to a vehicle geometry and a trajectory. If the trajectory obtained by the optimization is very dissimilar to the vehicle geometry used to generate the data, Missile DATCOM will have to be re-run for new aerodynamic coefficients.

V. Results

The optimization setup is used for 7 different designs (cases) and 6 different subcases. The cases identify different architectures, in number of stages, type of propulsion, dry mass scaling (rubber stretchable tanks or constant) and guidance strategy. The subcases identify choices in payload mass and redundancy policy and choice of avionics. The reader is referred to Ref. [9] for details on the cases and subcases. Table 1 summarizes the cases and Table 2 the subcases.

Table 1. Case Characteristics

	1a	1b	2a	2b	5	6	7
Stages	TSTO	TSTO	TSTO	TSTO	SSTO	SSTO	SSTO
Prop	Solid	Solid	Solid	Solid	Liquid	Liquid	Hybrid
Scaling	Rubber	Const.	Rubber	Const.	Rubber	Rubber	Rubber
Upper stage guidance	Guided	Guided	Unguided	Unguided	Guided	Guided	Guided

Table 2. Subcase Description

Subcase	OS mass	Avionics	Telecom
1	6.65 kg	Single string	Single string
2	10 kg	Redundant IMUs	Baseline redundant
3	14 kg	Redundant IMUs	Classical (Electra-Lite)
4	14 kg	Full redundant	Baseline redundant
5	17 kg	Full redundant	Classical (Electra-Lite)
6	20 kg	Full redundant	Classical (Electra-Lite)

Additional numerical data for the parameters presented in the previous sections is shown in Table 3.

Table 3. Parameters

Parameter	Value	Units
μ	4.282837e13	m^3/s^2
$\|\|\Omega\|\|$	7.088218e-5	rad/s
R_p	3396.2	km
Γ_{max}	20	deg
$\bar{q}_{max}^{MECO}$	2	kPa
θ_0	90	deg
ϕ_0	0	deg
h_0	-1	km MOLA
t_{launch}	1	s
h_{orbit}	400	km
e_f	0	-
i_f	45	deg

Figures 5-10 present optimal trajectory profiles for case 5 subcase 3, abbreviated case 5.3. Subcase 3 presents a good compromise between GLOM and functionality. These profiles illustrate how mass, altitude, ground track, dynamic pressure, and the thrust angles evolve throughout the trajectory. Note that subcase 3 is taken as the baseline subcase for all cases.

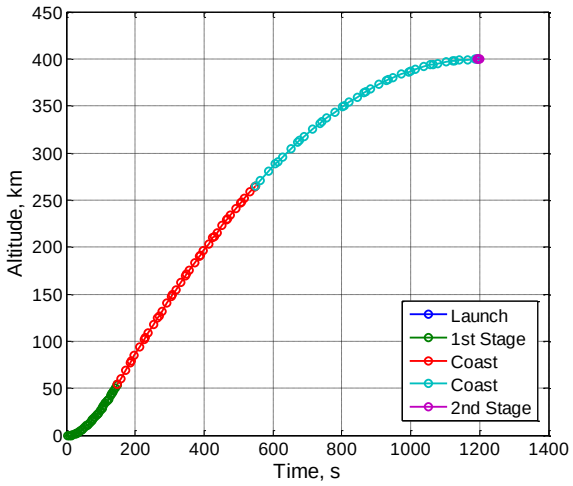

Figure 5. Altitude profile for case 5.3. *MECO happens at about 170 s, 50 km altitude.*

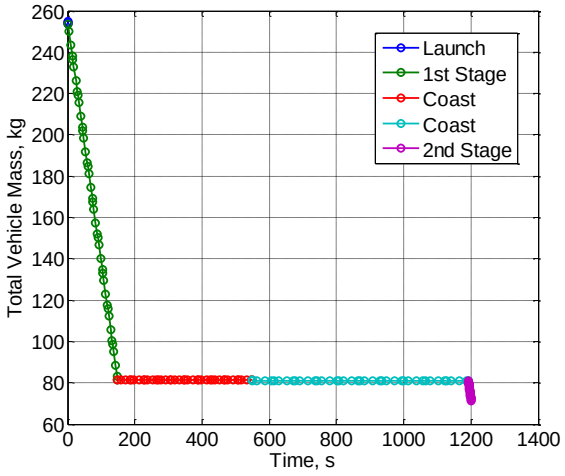

Figure 6. Total mass. *70% of the mass is lost during the first burn.*

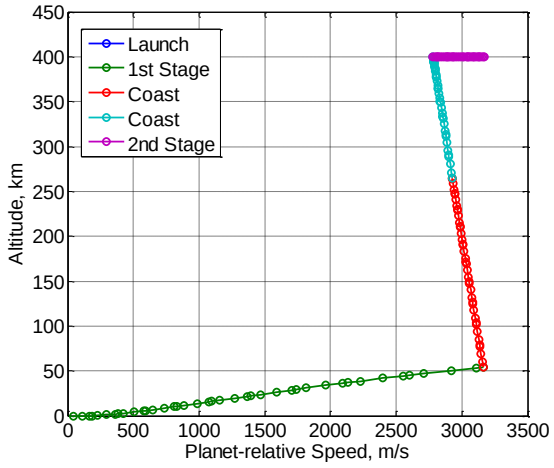

Figure 7. Altiude vs. Velocity. *Most of the ΔV is provided during the first burn.*

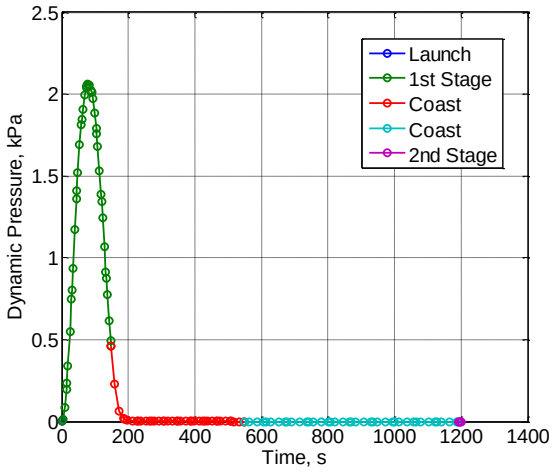

Figure 8. Dynamic pressure profile. *Although the peak dynamic pressure is about 2 kPa, by the MECO it is down to about 0.5 kPa*

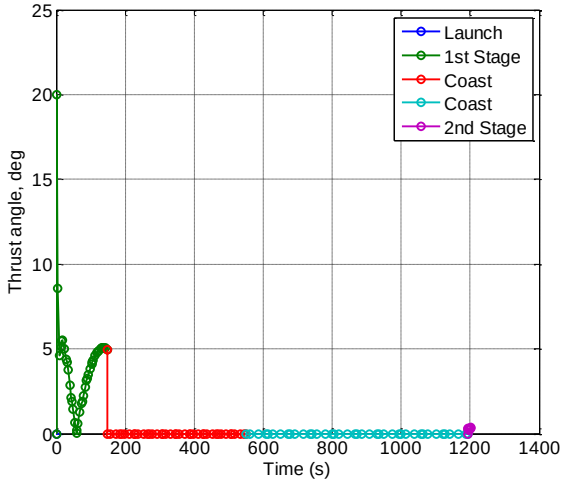

Figure 9. Thrust angle. *The thrust angle is maximum at the beginning of the first burn, bending the trajectory.*

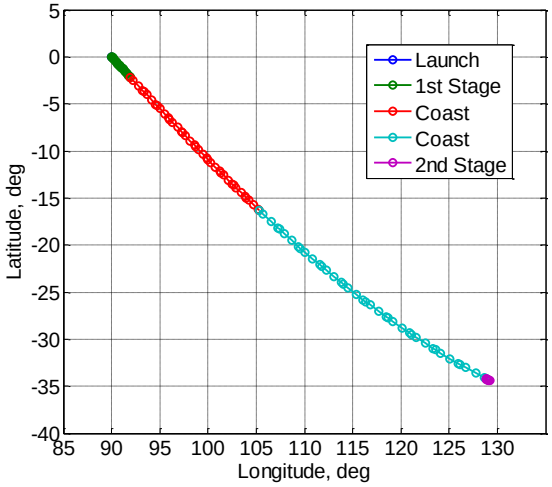

Figure 10. *Ground track. The total flown downrange is about 3000 km*

The baseline configuration comparisons (cases 1a.3 to 7.3) are presented in Figs. 11-16. From these results, it is shown that the lightest propulsion option is hybrid vehicle.

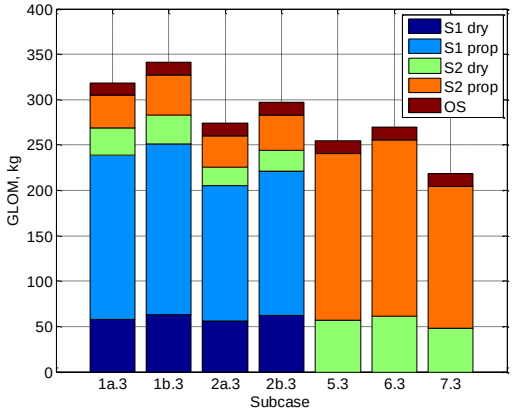

Figure 11. Total stack mass. *The lightest design is the hybrid. The TSTO, which are typically expected to be lightest, show as the heaviest, due to their low propellant mass fractions.*

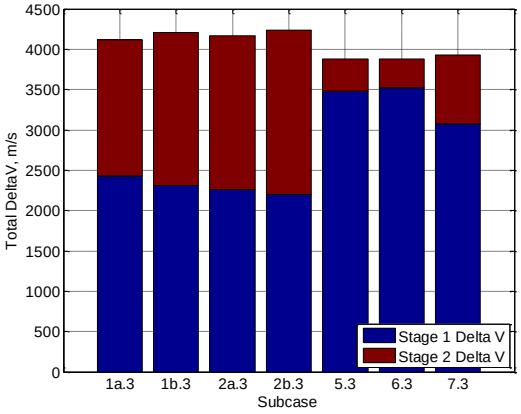

Figure 12. Propulsive ΔV. *The ΔV split clearly shows the differences between SSTO and TSTO architectures. Since SSTO designs have a very low propellant mass fraction before the second burn, the optimal design minimizes the size of the second ΔV, which is accomplished by flying a shallow trajectory. A shallower trajectory, with lower gravity losses, has also lower total ΔV.*

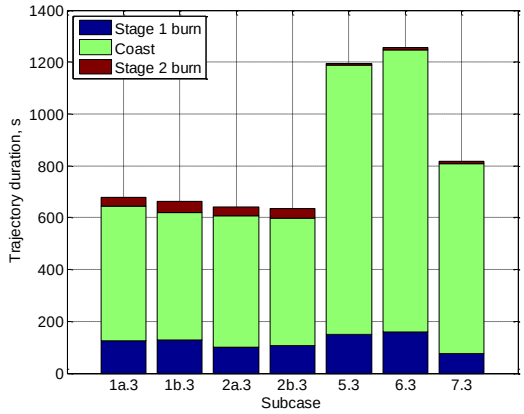

Figure 13. Trajectory duration. *SSTO architectures have much longer trajectories, due to a shallower profile.*

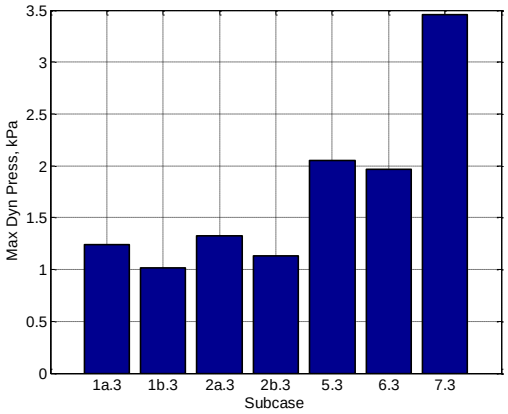

Figure 14. Maximum dynamic pressure. *The peak dynamic pressure is larger for the SSTO, due to a lower trajectory and larger first burn ΔV. The hybrid presents the largest thrust to GLOM ratio and therefore the largest peak dynamic pressure.*

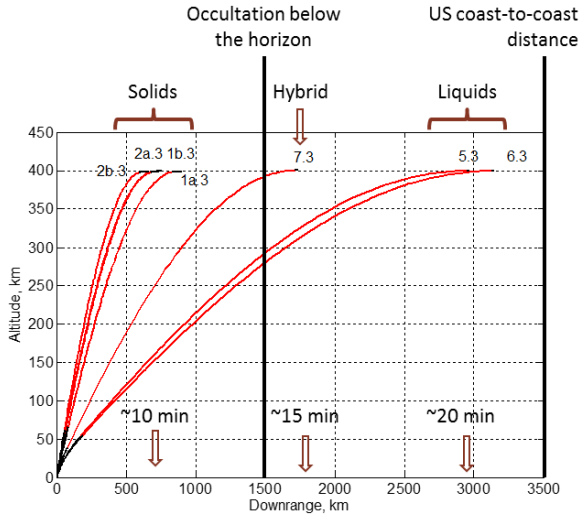

Figure 15. Downrange vs. altitude profiles for all baseline cases. *Although the hybrid is expected to have a profile similar to cases 5 and 6, the constrain on maximum dynamic pressure at MECO is active and forces the trajectory to be steeper.*

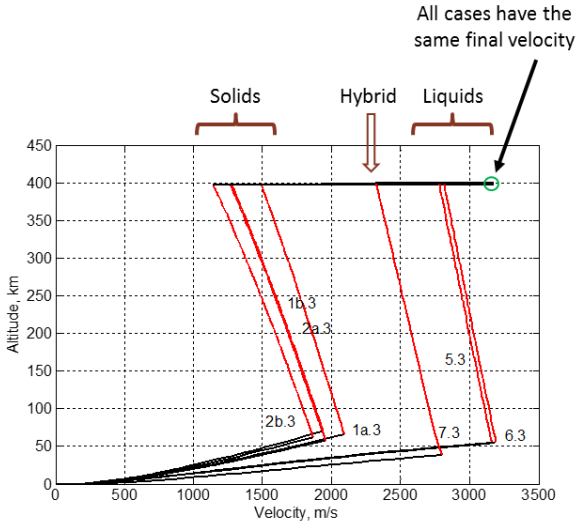

Figure 16. Altitude vs. velocity. *SSTO vs. TSTO designs present different altitude vs. velocity profiles. TSTO designs lose more velocity during coast and have a much larger stage 2 ΔV than the SSTO designs.*

VI. Sensitivity Analysis

A study was performed to evaluate the sensitivity of certain design parameters to some of the output variables, comparing case 2.3 and 5.3 (TSTO vs SSTO). The impact on GLOM is presented in Figures 17-20.

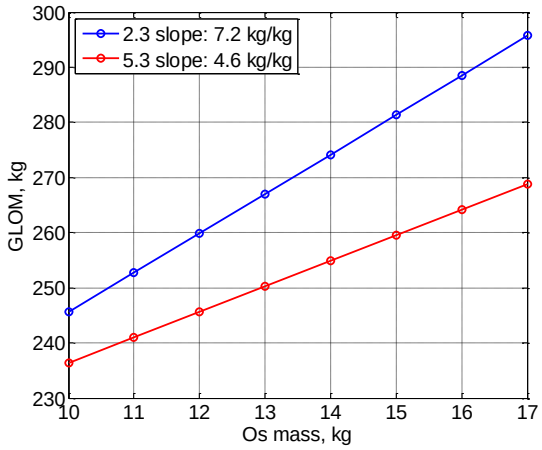

Figure 17. GLOM sensitivity to OS mass.

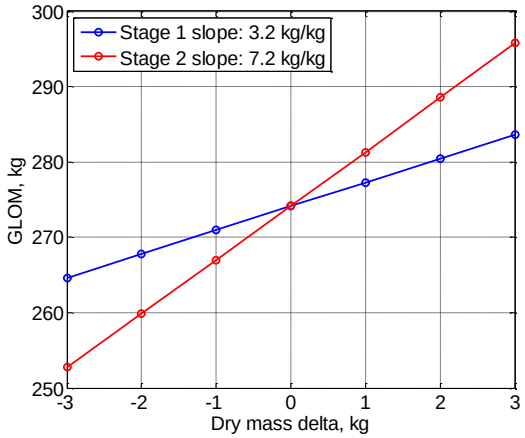

Figure 18. GLOM sensitivity to dry mass increments per stage (case 2.3 only).

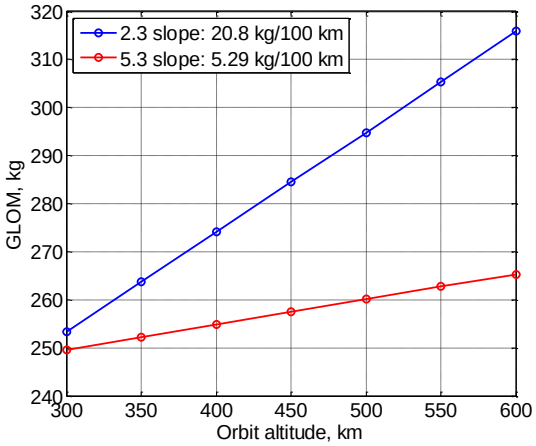

Figure 19. GLOM sensitivity to target orbit altitude.

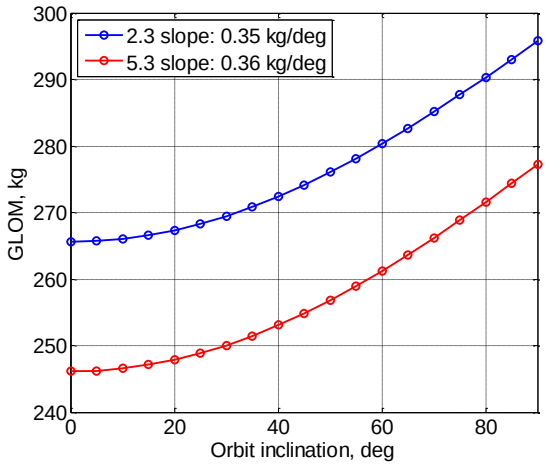

Figure 20. GLOM sensitivity to orbit inclination.

VII. Conclusion

This paper describes the approach based on trajectory optimization using GPOPS-II to design and characterize the option space for a MAV. The problem formulation, vehicle and design constraints and models used are outlined, and results for representative cases and subcases are presented. Additionally, a sensitivity analysis of variables of interest is introduced, with the objective to develop rules of thumb to aid mission and vehicle design. The reader is referred to Ref. [9] for additional information and consequences of the results presented in this paper.

Acknowledgements

The research was carried out at the Jet Propulsion Laboratory, California Institute of Technology, under a contract with the National Aeronautics and Space Administration. The authors thank the Mars Exploration Program Office for funding this project.

References

[1]Lu, P., Sun, H., and Tsai, B., ”Closed-Loop Endo-Atmospheric Ascent guidance,” AIAA paper 2002-4558, AIAA GNC Conference, Monterey, California, 2002.

[2]Dukeman, G., “Atmospheric Ascent Guidance for Rocket-Powered Launch Vehicles,” AIAA paper 2002-4559, AIAA GNC Conference, Monterey, California, 2002.

[3]Seywald, H., Cliff, E., "Neighboring Optimal Control Based Feedback Law for the Advanced Launch System," JGCD, Vol. 17, No. 6, pp. 1154-1162, 1994.

[4]McHenry, R. et al., "Space Shuttle Ascent Guidance Navigation and Control," Journal of the Astronautical Sciences, Vol. 27, No. 1, pp. 1-38, 1979.

[5]Patterson, M., and Rao, A., "GPOPS-II: A MATLAB Software for Solving Multiple-Phase Optimal Control Problems Using hp-Adaptive Gaussian Quadrature Collocation Methods and Sparse Nonlinear Programming," ACM Transactions on Mathematical Software, Vol. 41, Issue 1, October 2014.

[6]Coskun, E., "Multistage Launch Vehicle Design with Thrust Profile and Trajectory Optimization," PhD thesis, Middle East Technical University, 2014

[7]Mars Global Reference Atmospheric Model http://see.msfc.nasa.gov/tte/model_Marsgram.html

[8]Rosema, C. et al., "Missile DATCOM User's Manual," Air Force Research Laboratory, 2011

[9]Shotwell, R. et. al., "Drivers, Developments and Options under Consideration for a Mars Ascent Vehicle," IEEE Aerospace Conference, 2016.